RESEARCH PAPER

Controlling root penetration in electron beam welding by a through-current feedback

Miikka Karhu[1] · **Veli Kujanpää**[1]

Abstract

Electron beam (EB) welding is a keyhole welding process in which the kinetic energy of focused electrons is converted into the heat required for welding. When a full penetration weld is achieved in keyhole EB welding, a small part of the electrons from the electron beam pass through the workpiece via the open keyhole at the root side of the weld. These electrons provide a charge whose current value can be measured, namely, the through-current. The aim of this study was to develop and build a control system integrated in the EB welding machine that enables the maintenance of complete root penetration in EB welding by means of an adaptive control system. The adaptation was performed with closed-loop feedback equipment that simultaneously measures the electrons passing through the workpiece via the keyhole (transmitted through-current) and adjusts the required beam current parameter relative to the through-current measured during welding. The results of the welding tests demonstrated the functionality of the developed control system and the suitability of the concept itself. For example, in a welding test run in which the thickness of the test piece was linearly increased from 10 to 12 mm, the control system was able to react and regulate the welding power required for complete root penetration along the whole thickness range. In the above case, the test results showed that based on the measured through-current data, the control system instantaneously increased the amount of beam current required during welding linearly with increasing thickness of the plate to be welded.

Keywords Electron beam welding · Keyhole · Through-current · Beam current · Weld root penetration · Austenitic stainless steel

1 Introduction

Electron beam (EB) welding is an automated and computer-controlled fusion welding process that is typically performed in a vacuum environment in the working chamber of an EB welding machine. A more in-depth description of the principles associated with EB welding, referred to in the following simplified description, can be found in [1–3]. The generation

---

Miikka Karhu and Veli Kujanpää both authors were formerly with VTT Technical Research Centre of Finland.

✉ Miikka Karhu
  miikka.karhu@lut.fi

  Veli Kujanpää
  veli.kujanpaa@lut.fi

1 Laboratory of Welding Technology, LUT University, Yliopistonkatu 34, 53850 Lappeenranta, Finland

---

of the electron beam takes place in a high vacuum environment in an electron beam gun, where electrons are emitted from the cathode to the anode by heating the cathode with a high voltage source. The emitted electrons are accelerated between the cathode and the anode to a speed that reaches 2/3 of the speed of light and are then focused into a beam shape by means of an electromagnetic coil. The accelerated and focused electron beam has such a large kinetic energy applied to a small area that when the electron beam hits the workpiece surface, its power density ($> 10^6$ W/cm^2) is sufficient to form a keyhole in the material to be welded. In other words, the kinetic energy of the electrons at the point of impact is converted into heat, which melts and vaporizes the material locally and finally forms a vapor channel surrounded by the molten envelope. When either the electron beam or the workpiece to be welded is moved relative to each other, the keyhole in the workpiece moves in the welding direction and the molten material around the keyhole flows backward to form a trailing melt pool that solidifies during welding movement and forms a weld.

EB welding is a versatile process when looking at material thicknesses and materials suitable for welding. With high-power EB welding equipment (power level up to 100 kW or more), a weld joints up to several hundred millimeters thick can be welded in a single pass. On the other hand, welding of very thin films, where the thickness of the materials to be joined can be tenths of a millimeter, is also possible [3–6]. EB welding can be used to join materials that are difficult or impossible to weld by conventional arc welding methods. In such cases, the properties of the material can be listed as high thermal conductivity, high melting point, sensitivity to react with atmospheric gas molecules at elevated temperature. Such materials, where the advantages of the EB welding process allow a successful welding result, include for example copper, titanium, tantalum, niobium, zirconium, and alloys thereof [1, 3, 6–10]. The advantages of EB welding have proven it to be a manufacturing method that has been successfully utilized in components or products for a variety of applications, such as aerospace, medical, transportation, and energy production [1, 3, 11–17]. One major EB welding application related to the power generation industry, to which the application of this study is related, is the fabrication and assembly of components for large thick-walled pressure vessel structures required in power plants. EB welding is an attractive process option in the assembly production of the abovementioned components and structures, as it can achieve faster production times as well as significantly lower weld deformations and enables more precise manufacturing tolerance requirements to be met compared to, for example, traditionally used arc welding processes such as gas metal arc welding and narrow-gap gas tungsten arc welding [18–24].

Even though EB welding can be considered a fully automated process, research and development work has been done over the years to improve and ensure control of the process during welding. The augmentation of controlling operations is related, for example, to the strict alignment and positioning requirement of the electron beam in relation to the location of the joint/groove to be welded. In references [25–32], it can be found various alternatives introduced in detail for systems where the focal position of the electron beam in relation to the workpiece and the joint to be welded can be controlled in real time. The information for the control system needed for control and adjustment during the welding process is obtained by using suitable sensors that are able to collect, for example, the secondary current in plasma from the weld plume, the intensity of backscattered electrons/X-rays from the welding direction. In the abovementioned cases, the sensors needed are placed above the weld at the area of interaction between the electron beam and the workpiece during welding. Mentioned monitoring information in the above systems can also be used as output information for the joint tracking control signals of the control system, which adjust the correct position/track in relationship between the beam and the joint during welding. Furthermore, in reference [33], it is presented a method which is proposed for determining the degree of weld penetration during welding by measuring the X-ray radiation form the rear side of the weld.

The need for this research has arisen from the development work of quality control for EB welding of the previously mentioned massive thick-walled vessel structures. One of the challenges to be considered in quality assurance in the welding of these structures is that in certain assembly welds it is only possible to weld on one side and visual and X-ray inspection is not always possible on the root side due to geometric constraints. Another factor affecting the quality of the root side of the weld is related to the possible variation in the joint thickness of the structure to be welded. The thickness variation may be appropriate based on the design, or it may be the variation allowed by the manufacturing tolerances. In extreme cases of joint thickness variations, to ensure a high-quality welding result, it may be necessary to adjust the welding parameters in real time during welding to ensure complete penetration and the quality of the root side of the weld. In this particular case, it is necessary to control the welding power (by adjusting the beam current) to ensure proper fusion depth of the weld and root formation in order to avoid incomplete root penetration, root concavity, or lack of root fusion defects. It has therefore been seen that it is necessary to develop the control of the welding process used to such a level that the uniform quality of the weld and the penetration of the root side can be maintained and ensured during the welding of the structures in question.

An electron beam consists of electrons that have an electric charge, and as a result of this charge and the movement of electrons, a beam current (mA) is generated. The product of the beam current (mA) and the acceleration voltage (kV) determines the beam power (kW) available for welding. The magnitude of the beam power used determines, e.g., the penetration depth to be achieved in the weld. In practice, the beam power (welding power) of the process is controlled by changing the beam current, while the acceleration voltage is normally kept constant. In keyhole EB welding, where a stream of electrons is first applied to the surface of the workpiece in the form of a focused electron beam, most of the beam current is conducted to the workpiece and get grounded, while a small portion passes through the workpiece through an open keyhole. These through-transmitted electrons provide a charge whose current value can be measured, and it is called a through-current. Preliminary studies related to this work had found a good correlation between sufficient through-current and complete root penetration of the weld. This background information was utilized in this

study. According to the literature research conducted by the authors, similar studies conducted by another research unit or researchers have not been published before. Thus, the authors would see the research results discussed in this study is bringing new value to EB welding and further strengthening and expanding the usability of EB welding as both a high quality and efficient manufacturing process option in industrial applications.

2 Materials and methods

The base materials used in the welding experiments were two different austenitic stainless steels. The material thicknesses of the test pieces ranged from 7 to 14 mm. The material used for the test pieces with material thicknesses of 7 mm was AISI 316LN (EN 1.4406), while the material used for the other test pieces and material thicknesses was AISI 304L (EN 1.4307). The chemical compositions of the materials can be seen from Table 1.

As shown in Fig. 1, the electron beam welding machine used in the welding experiments was a Leybold Heraeus 1001/15–150-CNC. The maximum power of the electron beam gun is 15 kW, and it is based on an acceleration voltage of 150 kV and a beam current of 100 mA. The beam handling system is equipped with function generation that allows for different beam oscillations. The volume of the vacuum chamber is 1.4 m^3 (length 1.4 m, height 1.115 m and width 0.9 m). The machine is NC-controlled with a 3 + 1 axis and welding movements can be performed with manipulators such as using an *X/Y*-motion table and/or rotary units. For the welding tests, the working chamber was depressurized with the vacuum pump system of the EB welding machine. The vacuum pump system consisted of both mechanical and kinetic pumps, which made it possible to achieve the desired vacuum level.

2.1 Experimental procedure

The experimental work was divided into two phases. In phase 1, a proper measurement system for measuring the current caused by electrons passing through the workpiece during welding was developed and built. In that phase 1, preliminary welding tests were performed to map the sensitivity of the data acquisition process and to ensure the functionality of the measurement system. The actions in phase 2 were based on the promising results of the preliminary welding

Fig. 1 Electron beam welding machine employed in the welding experiments

tests performed in phase 1. During phase 2, the measurement system was upgraded by building a closed-loop adaptive control connection to the system. As the last part of phase 2, welding tests were performed to ensure the performance and usability of the developed control system.

The welding experiments to test the functionality of the measuring system in phase 1 were carried out in a flat position and with bead-on-plate weld runs. The length of the test welds was 170 mm. The thicknesses of the welded specimens were 7, 10, and 14 mm, which were intended to simulate different depths of joint options. The welding parameters for each material thickness in phase 1 are shown in Table 2.

The welding experiments to test the performance and usability of the developed control system in phase 2 were carried out in a flat position and with bead-on-plate runs. The length of test welds was 170 mm. At first, some preliminary test welding was performed with a plate thickness of 10 mm to find welding parameters that provide complete penetration depth

Table 1 Chemical compositions of test materials

Element weight-%	C	Si	Mn	P	S	Cr	Ni	Mo	N	Fe
AISI 316LN	0.017	0.40	1.20	0.031	0.001	17.2	12.4	2.59	0.17	Balanced
AISI 304L	0.017	0.33	1.52	0.025	0.000	18.2	8.2	-	0.07	Balanced

and proper contour for the root side. In practice, this meant that by experimenting the welding speed range and beam oscillation, root side of the weld was tried to produce wider and thus smoother. After the welding tests performed on mentioned preliminary test samples, the test pieces were machined with varying material thicknesses for the actual welding tests to be performed in phase 2. The longitudinal cross-sections of those test pieces (test piece 10D12 and 10D8) can be seen in Fig. 2. The purpose of the welding tests of phase

Table 2 Welding parameters for different material thicknesses used in the experiments of phase 1

Constants	Variables
Welding parameters for material thickness of 7 mm (test pieces A7 and B7)	
- Acceleration voltage: 150 kV - Working pressure: 10^{-3} mbar - Working distance: 529 mm - Welding speed: 800 mm/min - Oscillation: $xy = 1.5$ mm - Lens current: 493 mA	- Beam current: 23.5 mA (test piece A7) - Beam current: 12.7 mA (test piece B7)
Welding parameters for material thickness of 10 mm (test pieces A10 and B10)	
- Acceleration voltage: 150 kV - Working pressure: 10^{-3} mbar - Working distance: 526 mm - Welding speed: 800 mm/min - Oscillation: $xy = 0.5$ mm	Test piece A10 - Beam current: 39 mA - Lens current: 489 mA Test piece B10 - Beam current: 26 mA - Lens current: 484 mA
Welding parameters for material thickness of 14 mm (test pieces A14 and B14)	
- Acceleration voltage: 150 kV - Working pressure: 10^{-3} mbar - Working distance: 522 mm - Welding speed: 800 mm/min - Oscillation: $xy = 0.5$ mm - Lens current: 483 mA	- Beam current: 52.3 mA (test piece A14) - Beam current: 45.5 mA (test piece B14)

Fig. 2 The longitudinal cross-sections of the test pieces used in the welding tests of phase 2. Above: (1) test piece 10D12. Below: (2) test piece 10D8. The units in the figure are in millimeters
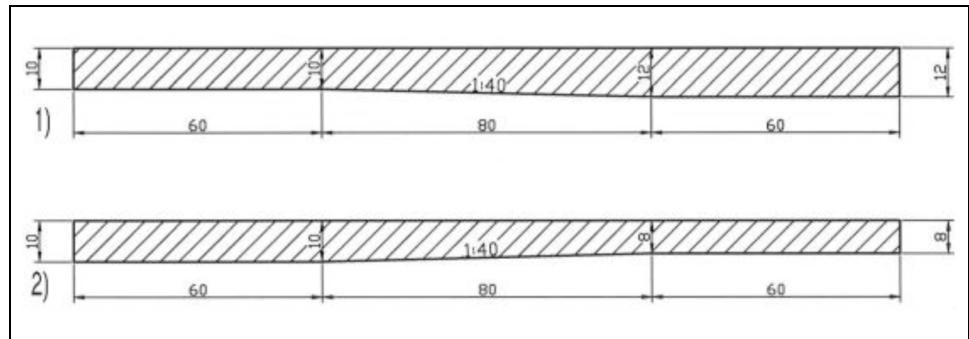

Table 3 Welding parameters used in the experiments of phase 2

Welding parameters	
Constants	Variables
- Acceleration voltage: 150 kV - Working pressure: 10^{-3} mbar - Working distance: 422 mm - Welding speed: 650 mm/min - Oscillation: $xy = 2.3$ mm - Lens current: 502 mA (-5 mA below of focal point's surface value) - Through-current set value: 3.0 mA	- Beam current value adjusted by the control system connected to the EB welding machine

2 was to determine if the control system could react and function properly when the thickness of the material to be welded changes during welding. The welding parameters used in the phase 2 welding tests are shown in Table 3.

Evaluations of the experimental results were performed by visual inspection of the welded specimens and welding data derived from the computer (PC system) data acquisition (DA) unit. After the welding tests, through-current data obtained from the PC data acquisition unit were converted into charts using a spreadsheet program. The amount of through-current and beam current of the EB gun in milliamperes (mA) were plotted separately on the vertical axis, while the elapsed time of the welding cycle in milliseconds (ms) was displayed on the horizontal axis. The root of the weld of the specimens were also photographed and cross-sectional macro graphs were selectively made from the test welds.

2.2 Description of the measuring/control system used in the welding experiments

The developed control system is based on the following factors that come from the nature of the EB welding process. Electron beam is formed from electrons, which possess an electrical charge and as a resultant of this charge and a movement of electrons, the beam current is formed. The product of beam current (mA) and acceleration voltage (kV) determines beam power (kW) which is available for welding. The used magnitude of beam power defines, e.g., the attainable depth of penetration. In practice, beam power of the process is adjusted with altering the beam current, while acceleration voltage is normally kept constant. When contemplated in a reduced manner the full penetrating welding sequence on behalf of beam current, at first comes impinging beam current as a form of focused beam to the surface of the work piece. After that, most of the beam current is conducted into a work piece and got grounded, whereas a small proportion is transmitted through the work piece via an open keyhole (through-current).

Under the circumstances, there was a need to develop and build a suitable system which measures the through-current as input and can respond instantaneously (in tens of milliseconds) to the through-current changes by adjusting the beam current according to this feedback. A principal illustration of measurement system configuration is shown in Fig. 3. A through-transmitted electrons (through-current) collecting detector made of a 5-mm-thick copper plate is situated approx. 10 mm under the work piece to be welded. The detector is insulated from the working table with using ceramic insulators and wired to the PC system.

Required data acquisition hardware to PC was purchased from National Instruments, which is also distributor for LabVIEW programming language used in software development. The measuring and control functions were realized with LabVIEW program. With the modular programming concept, it is relatively easy to generate PC-based measuring and control applications with handy user interfaces. The principle of the program flow of the measurement and control functions of

Fig. 3 Principle configuration of the measurement system connected to the EB welding machine
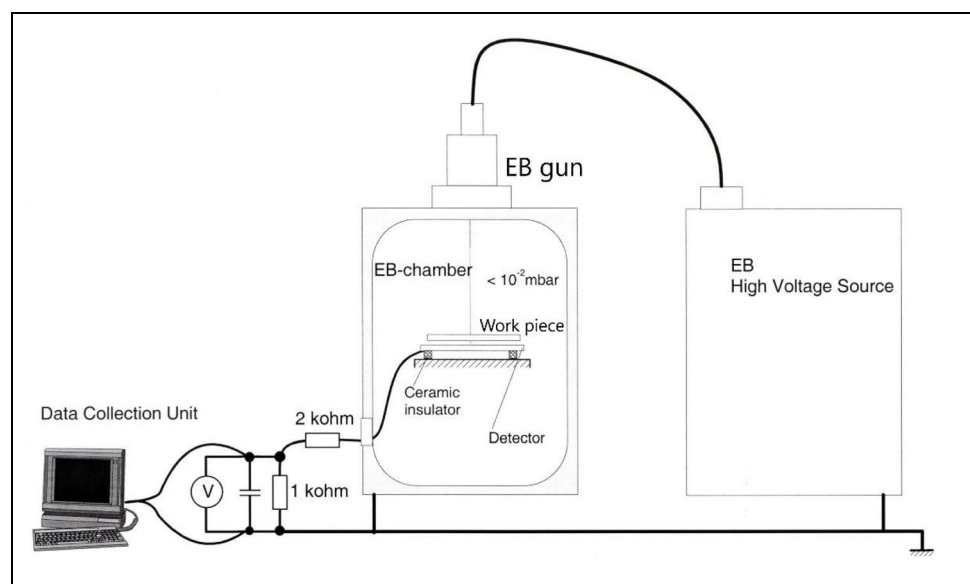
the equipment developed in the study can be outlined as follows:

- Immediately after the program starts, the parameter file is red, and values set for the corresponding welding variables.
- Program checks that cabling is OK and an external + 24 V source is connected. If not, it will exit and inform the user about the error source.
- Relay R1 is turned on, which will switch the welding beam current control of the EB from the potentiometer to the PC control.
- Program will wait until the "START-welding" button of the EB welding machine is pressed.
- Control loop is started and running at 50 Hz frequency:

Read a value from DAQ card's A/D

Scale the value from voltage [V] to through-current [mA]

Take the value to the chart (plots through-current behavior on PC's display)

Calculate PI-algorithm

Limit the value to ramp (a control algorithm implemented to prevent too fast current rise)

Scale the output (current request to EB) from [mA] to [V]

Take the value to D/A-converter of the DAQ card and plot the control voltage behavior on PC's display

The control voltage from PC-DAQ (Data AcQuisition card) to EB welding machine (EBWM) is fed through a signal isolator to protect both the EBWM and PC-DAQ. The relay is also inherently isolating, so the analog and digital control signals between EBWM and PC are galvanically isolated. The control algorithm used in this application is basic proportional integral (PI) controller. The P-part of the controller calculates the difference of set value and current value and multiplies it with P-multiplier. The I-part sums the long-term differences (of the set and measured values) from sample to sample, multiplies the sum with I-multiplier, and adds it to the output of the P-part. This sum is then scaled and output to the EBWM as a new welding beam current value.

The welding operator can set the desired through-current rate in advance of welding from the PC display in a purpose-tailored program menu. During welding, the stream of electrons coming through the keyhole impinge to the surface of the copper detector located underneath the work piece and in the form of transmitted current (through-current in mA) and the PC system records it as an input data. The control system simultaneously uses the input data to adjust the electron beam gun, which regulates the beam current.

Abovementioned action sequences will run in a closed-loop during welding. The purpose is that when the thickness of the joint to be welded changes during welding, the control system adjusts the value of the beam current and with it the welding power on the basis of the through-current measurement data, thus ensuring the complete weld penetration.

3 Results and discussion

3.1 Phase 1—Preliminary welding tests of measuring system

In phase 1, preliminary welding tests were performed to determine the sensitivity of the welding process with respect to the quality of the full penetrated weld root and the required through-current rate, as well as to ensure the functionality of the measurement system. The thicknesses of the welded specimens were 7 mm, 10 mm, and 14 mm, which were intended to simulate different depths of joint options.

In Fig. 4, it is shown the bead-on-plate welding data for the 7-mm-thick test pieces (A7 and B7) in terms of through-current during welding. The amount of through-current is plotted on the vertical axis, while the elapsed time of the welding cycle in milliseconds (ms) is displayed on the horizontal axis.

Figure 4 shows two through-current curves in which the test piece A7 was welded with a beam current of 23.5 mA, while B7 was welded with a beam current of 12.7 mA. In the welding of test pieces A7 and B7, the average
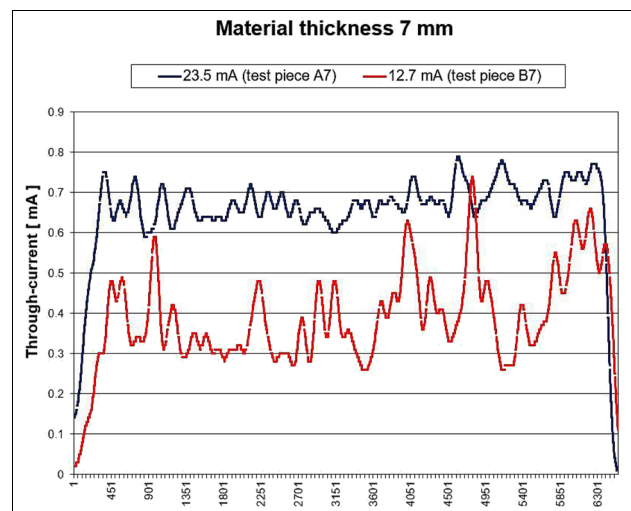

Fig. 4 Through-current data from bead-on-plate welding experiments with 7-mm-thick test pieces A7 (curve in dark blue) and B7 (curve in red). The elapsed time of the welding cycle in milliseconds (ms) is displayed on the horizontal axis

Fig. 5 Bead-on-plate weld of a 7-mm-thick test piece A7: **a**) root side of the weld and **b**) macro cross-section. Beam current used: 23.5 mA. In the scale strip, one interval corresponds to 1 mm
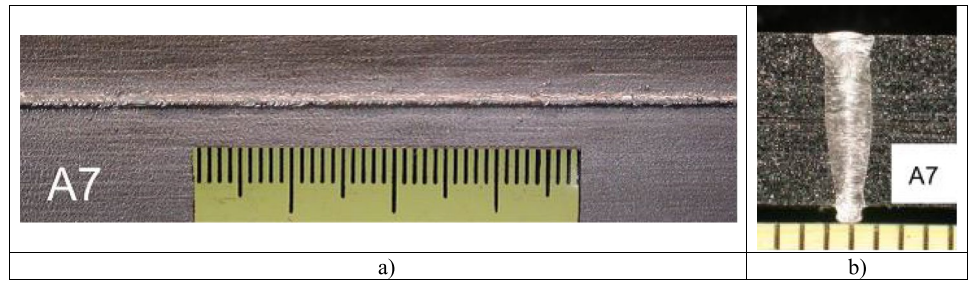

a)

b)

Fig. 6 Root side appearance of bead-on-plate weld of a 7-mm-thick test piece B7. Beam current used: 12.7 mA. In the scale strip, one interval corresponds to 1 mm
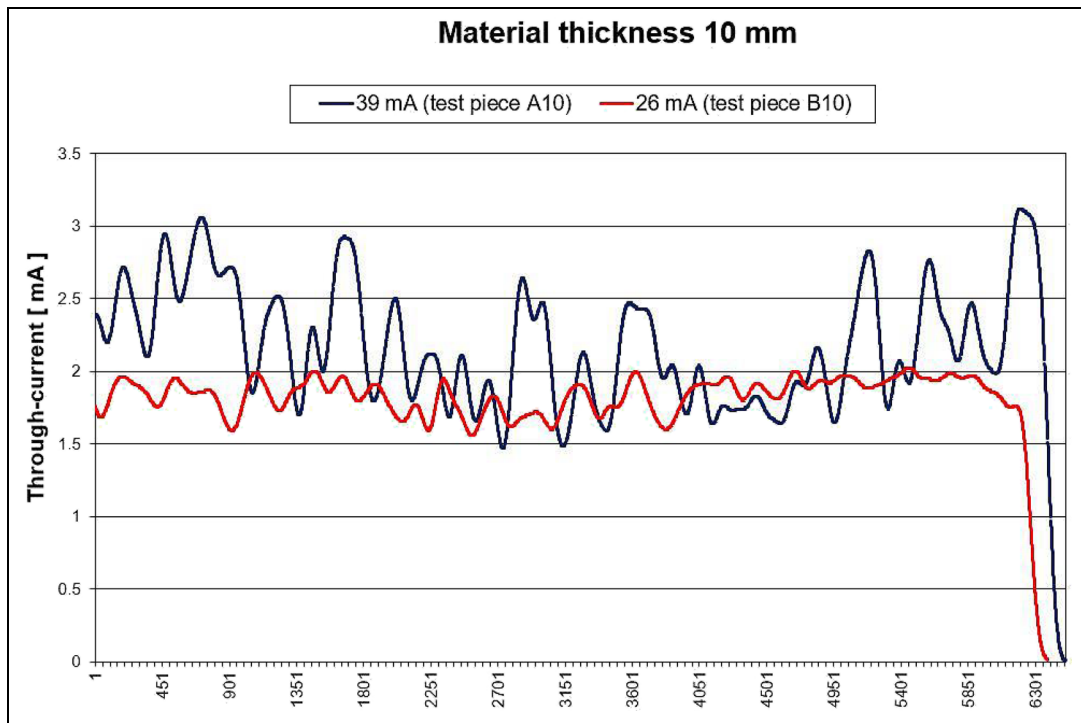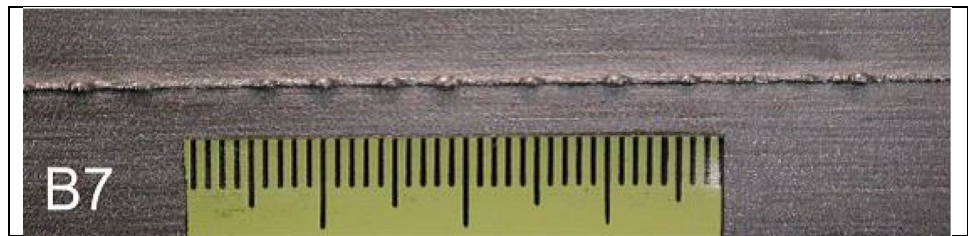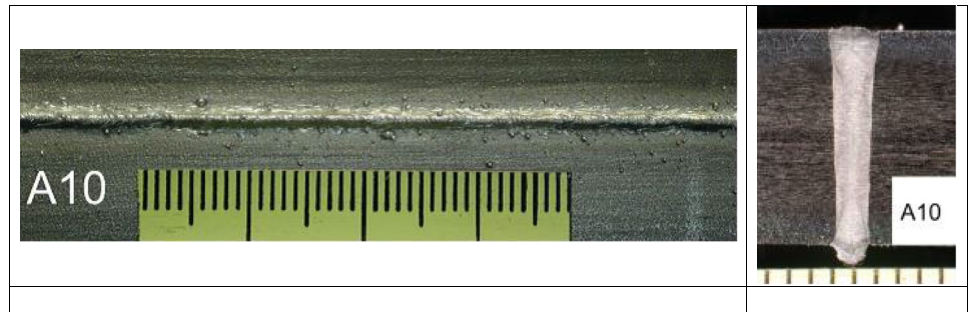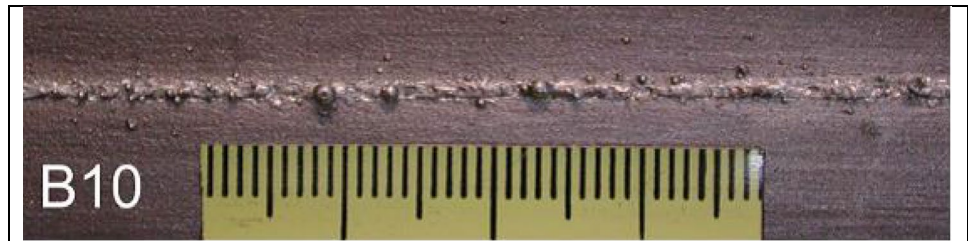

Fig. 7 Through-current data from bead-on-plate welding experiments with 10-mm-thick test pieces A10 (curve in dark blue) and B10 (curve in red). The elapsed time of the welding cycle in milliseconds (ms) is displayed on the horizontal axis

through-current was determined to be 0.62 mA and 0.37 mA, respectively. Figure 5a and b) shows the appearance from the root si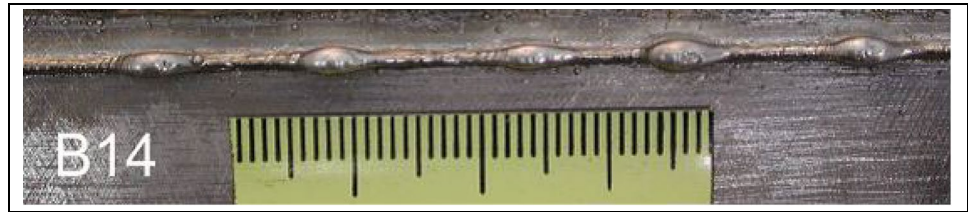de of the weld A7 and the macro cross-section, respectively. Figure 6 shows the appearance from the root side of the test weld B7.

In Fig. 7, it is presented the through-current curves of the bead-on-plate test welds of 10-mm-thick test pieces 10A and 10B. The test piece A10 was welded with a beam current of 39 mA, while B10 was welded with a beam current of 26 mA. In the welding of test pieces A10 and B10, the average through-current was determined to be 2.05 mA and 1.72 mA, respectively. Figure 8a and b) shows the appearance from the root side of the weld A10 and the macro cross-section, respectively.

Fig. 8 Bead-on-plate weld of a 10-mm-thick test piece A10: **a**) root side of the weld and **b**) macro cross-section. Beam current used: 39 mA. In the scale strip, one interval corresponds to 1 mm

Fig. 9 Root side appearance of bead-on-plate weld of a 10-mm-thick test piece B10. Beam current used: 26 mA. In the scale strip, one interval corresponds to 1 mm

Fig. 10 Through-current data from bead-on-plate welding experiments with 14-mm-thick test pieces A14 (curve in dark blue) and B14 (curve in red). The elapsed time of the welding cycle in milliseconds (ms) is displayed on the horizontal axis
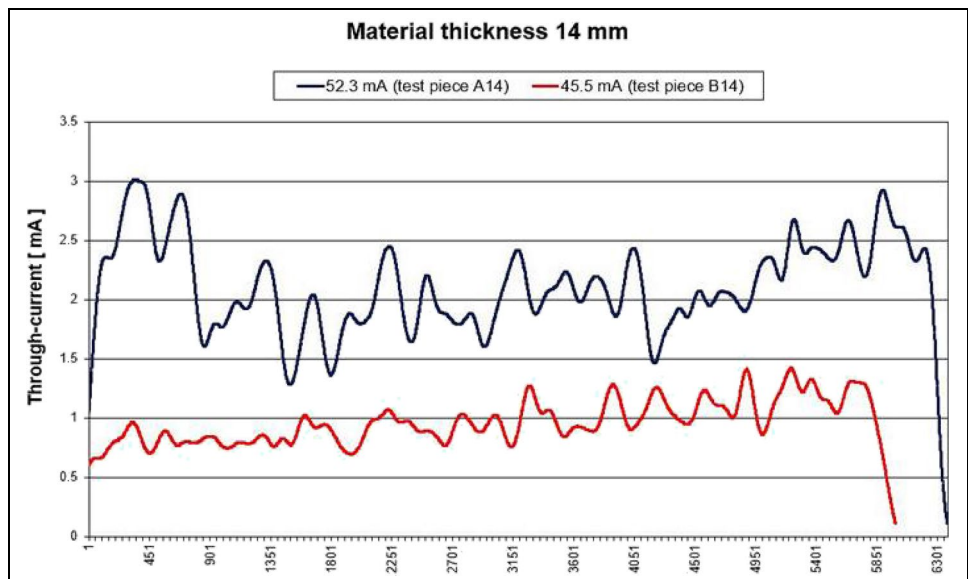
Fig. 11 Bead-on-plate weld of a 14-mm-thick test piece A14: **a**) root side of the weld and **b**) macro cross-section. Beam current used: 52.3 mA. In the scale strip, one interval corresponds to 1 mm

Fig. 12 Root side appearance of bead-on-plate weld of a 14-mm-thick test piece B14. Beam current used: 45.5 mA. In the scale strip, one interval corresponds to 1 mm

Figure 9 shows the appearance from the root side of the test weld B10.

In Fig. 10, it is presented the through-current curves of the bead-on-plate test welds of 14-mm-thick test pieces 14A and 14B. Test piece A14 was welded with a beam current of 52.3 mA, while B10 was welded with a beam current of 45.5 mA. In the welding of test pieces A14 and B14, the average through-current was determined to be 1.99 mA and 0.91 mA, respectively. Figure 11a and b) shows the appearance from the root side of the weld A14 and the macro cross-section, respectively. Figure 12 shows the appearance from the root side of the test weld B14.

Studying the behavior of the plotted through-current curves (Figs. 4, 7, and 10) obtained from the measurements, it can be seen that fluctuation, which is shown as peaks and valleys, occurs in all test welding result curves in both the A and B series. The fluctuating behavior of the through-current may be related to the dynamic behavior of the keyhole, in which the keyhole opening periodically widens and contracts during welding, with more electrons passing through the keyhole outlet during the expansion period and less during the contraction period.

When comparing the determined average through-current values to the corresponding weld penetrations and the success of the root formation of the weld, it can be seen that depending on the thickness of the plate to be welded, the average through-current value must exceed a certain threshold level to achieve complete weld penetration and proper root formation. For example, in the test welds B7, B10, and B14, the average through-current level remained too low, resulting in incomplete root penetration (Figs. 6 and 9) and uneven root side formation (Figs. 6, 9, and 12). Figures 6 and 12 show a typical bead necklacing-like defect in root formation resulting from an unstable keyhole when the flow of electrons passing through the root side (through-current) has not been sufficient to keep the keyhole opening sufficiently stable and the properly induced melt pool size on the root side. In contrast, for test welds A7, A10, and A14, the average through-current level has been sufficient to allow a stable keyhole and root side weld pool formation, resulting in complete weld penetration and evenly distributed root side formation (Figs. 5, 8, and 11).

The following correlation could be observed between the through-current and the complete root penetration of the joint thickness range under study: From the above results,

it can be concluded that for welding a material thickness of 7 mm, the default value level of the through-current should be at least 0.65 mA, while for material thicknesses of 10 mm and 14 mm, the default value should be at least 2 mA. It should be emphasized that the abovementioned default limits cannot be directly generalized but relate to the welding conditions described and the base materials used in this work. When different base material grades are used and changes in welding conditions and parameters are made, such as working pressure (vacuum level), working distance, and welding speed, they naturally affect the welding process and new through-current limits must be determined accordingly by pre-welding tests. As a whole, the performed welding tests confirmed that the built measuring system worked as planned. This was important information that led to the continuation of the research work to phase 2, where the control system unit was developed and integrated into the measurement system and subjected to performance tests.

3.2 Phase 2—Welding experiments to test the performance and usability of the developed control system

In phase 2, a closed-loop feedback control system was developed and connected to an EB welding machine. Welding tests were performed to ensure the performance and usability of the developed control system. The purpose was to investigate how well the measurement data can be used in EB welding for real-time control, where the developed control system adjusts the welding power (acceleration voltage is kept constant and beam current was used as a variable parameter) of the EB welding machine as the joint thickness increases or decreases, while maintaining the complete root side penetration during welding. Figure 13 shows a schematic representation of the execution of welding tests, including the welding start and finish points and the welding direction. Based on the results and experience of preliminary welding tests, the default through-current limit value for the control system was set to 3 mA. This means that during the welding of the test pieces, the control system receives information from the measuring system about the amount of through-current and adjusts the value of the beam current of the EB welding machine accordingly, with the aim of keeping the default through-current limit value at 3 mA level.
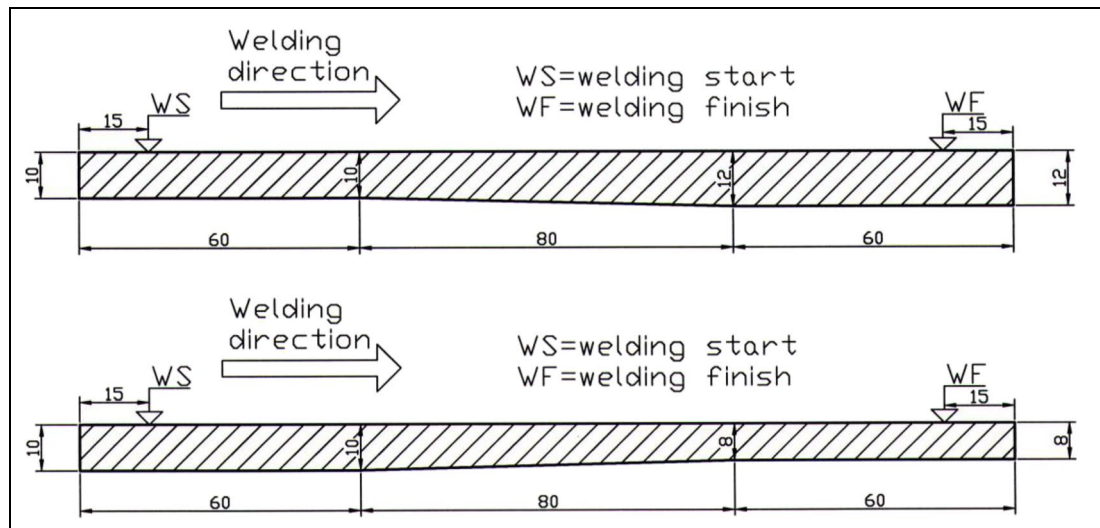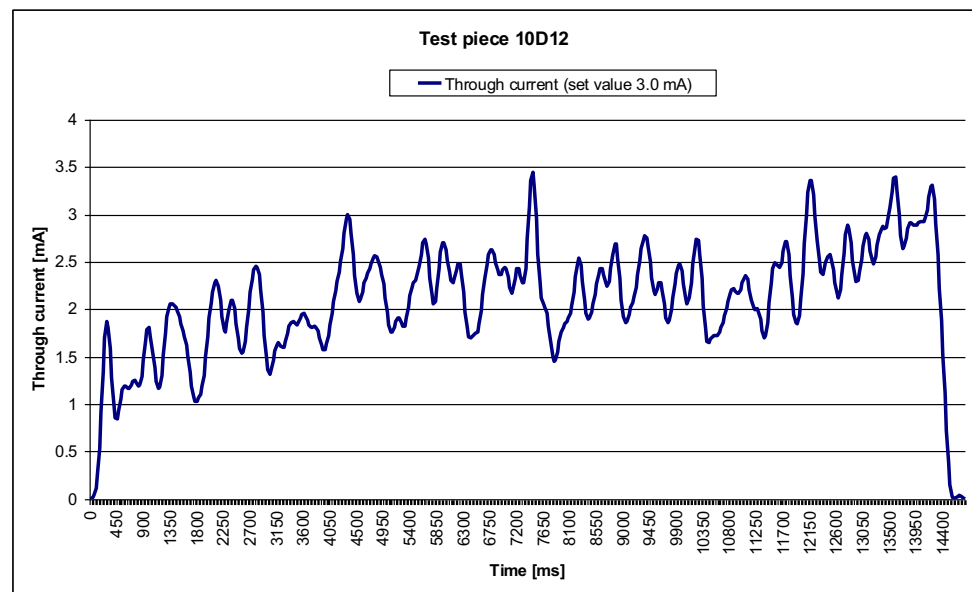
Fig. 13 Schematic showing the execution of welding experiments in which the thickness of the test piece (shown above) increased linearly from 10 to 12 mm (test weld 10D12) and (shown below) decreased linearly from 10 to 8 mm (test weld 10D8). The units in the figure are in millimeters

Fig. 14 Through-current data from bead-on-plate welding experiments of test piece 10D12

Figures 14, 15, 17, and 18 show the welding data of the test piece 10D12 and 10D8, respectively, as measured through-current and the beam current used during welding. The amount of through-current and beam current is plotted on the vertical axis, while the elapsed time of the welding cycle in milliseconds (ms) is displayed on the horizontal axis. In Figs. 16 and 19, it is shown the appearance from the root side of the weld and the weld macro cross-sections from test piece 10D12 and 10D8, respectively.

When evaluating the data material used to plot the curve in Fig. 15, it can be determined that the control system has increased the amount of beam current from 40 to 50 mA as the thickness of the welded specimen has increased from 10 to 12 mm. In other words, the beam power used in welding has also suitably increased from about 6.0 kW (= 40 mA × 150 kV) to 7.5 kW (= 50 mA × 150 kV) as the thickness of the test piece increases. In addition, the recorded data (plotted in Fig. 14) show that the average through-current value between the points where the thickness of the test piece 10D12 has increased from 10 to 12 mm is 2.2 mA, which is about 73% of the preset through-current value. Examining the appearance of the root side of the specimen 10D12 and the cross-sections

Fig. 15 Beam current data from bead-on-plate welding experiments of test piece 10D12. On the beam current curve, the locations of the beam current values that correspond to the values measured at points 1, 2, and 3 of the weld cross-sections (illustrated in Fig. 16) are marked with numbers
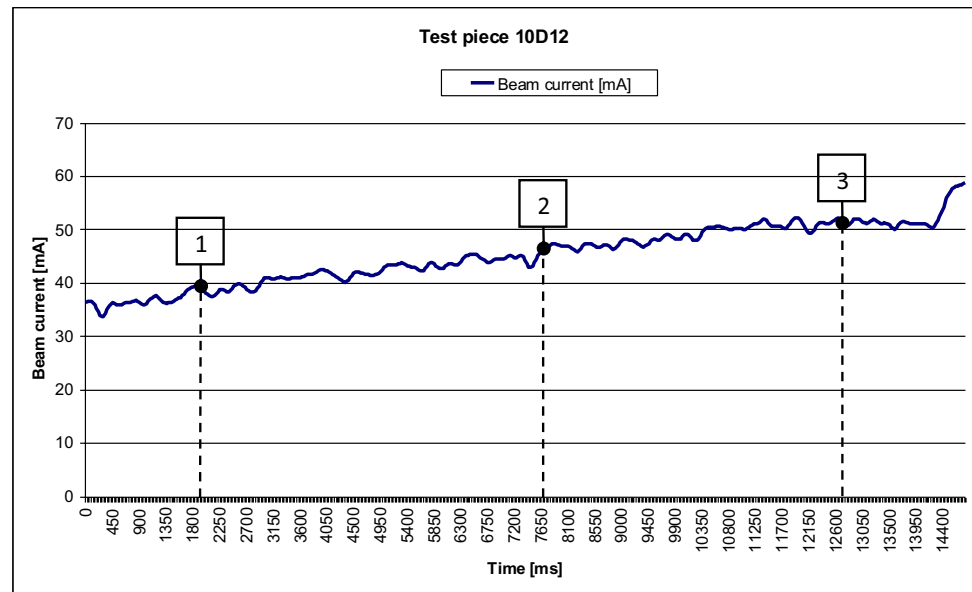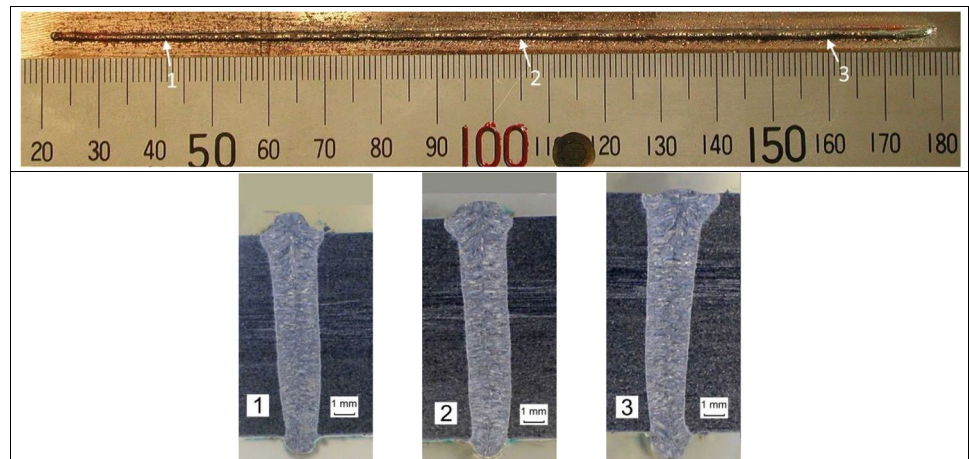

Fig. 16 Above: Appearance from the root side of test piece 10D12. Below: weld macro cross-sections from the test piece 10D12. Cross-Section 1 is taken from the front part (thickness = 10 mm) of test piece. Cross-Section 2 is taken from in the middle part (thickness = 11 mm) of test piece and cross-Section 3 is taken from the tail part (thickness = 12 mm)

of the weld (Fig. 16), it can be seen that the root of the weld is properly penetrated, and its appearance is smooth and continuous along the entire length of the root. Based on the above results, the control system proved to work as intended.

Figure 17 shows that the control system has kept the beam current values fairly constant during the welding of the test piece 10D8. The beam current values have remained at about 40 mA (corresponding to a 6 kW beam power level) as the thickness of the test piece has decreased linearly from 10 to 8 mm. The stored data (plotted in Fig. 18) show that the average through-current value between the points where the thickness has decreased from 10 to 8 mm is 2.8 mA, which is about 93% of the preset through-current value. When examining the penetration of the root side of the weld 10D8, it appears that reduction in the thickness of the plate in the range

used (from 10 to 8 mm) does not significantly affect the success of the welding result. The appearance of the root side of the test piece 10D8 in Fig. 19 confirms that the root of the weld is properly penetrated, and its shape is properly formed and continuous throughout the length of the root. This may be due to a suitably high through-current level (and beam current) used which expands the parameter window in which successful welding can be performed and thus, as the thickness of the test piece decreases, as in the above case, no significant changes in beam current are required.

In addition, the weld cross-sections of the test piece 10D8 (Fig. 19) show that there is a small undercut on the surface side of the weld. The observed undercut of the weld may be due to the astigmatism of the electron beam or a small perpendicular deviation of the horizontal plane of the test piece to the normal axis of the electron beam

Fig. 17 Beam current data from bead-on-plate welding experiments of test piece 10D8. On the beam current curve, the locations of the beam current values that correspond to the values measured at points 4, 5, and 6 of the weld cross-sections (illustrated in Fig. 19) are marked with numbers
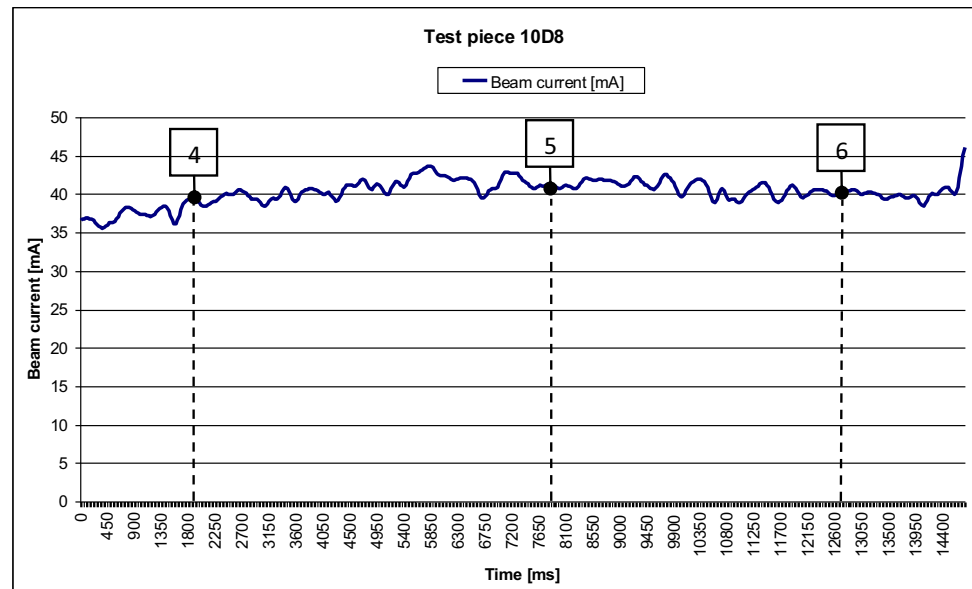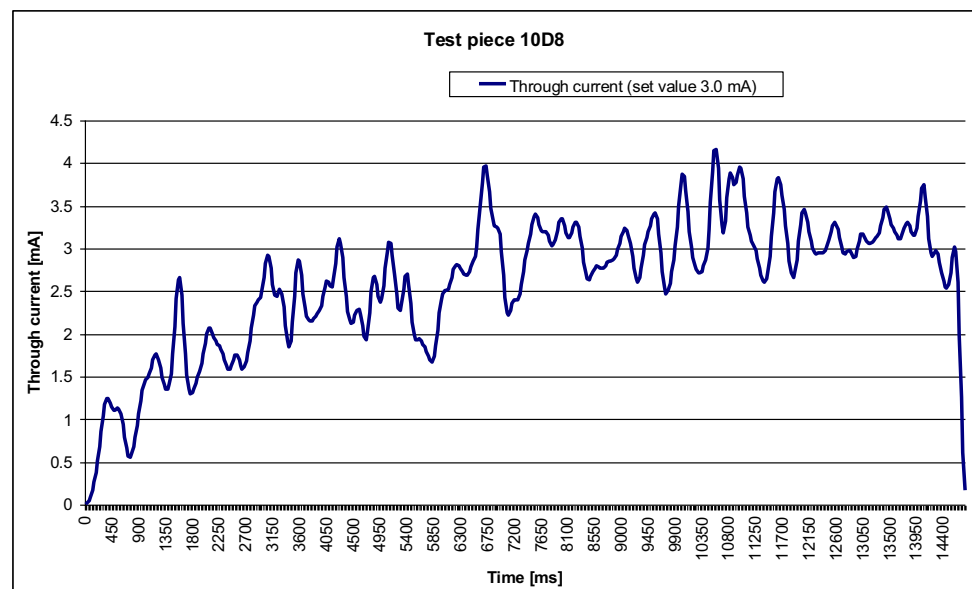

Fig. 18 Through-current data from bead-on-plate welding experiments of test piece 10D8


when the test piece is attached on a mounting table. The astigmatism of the electron beam may be due to a replaceable cathode strip filament that may have been worn into a replaceable condition.

The welding tests carried out as a whole gave promising results on the functionality of the control system and the suitability of the concept itself. However, further work is recommended, mainly to improve system reliability by collecting test data to validate adjustment limits (through-current vs. beam current) for welding tests using longer weld joints in conjunction with different welding positions and plate thicknesses.

4 Conclusions

During the work of this study, a closed-loop feedback control system was developed and connected to the EB welding machine. The principle of the control system was based on the measurement of the through-current formed by the electrons passing through the workpiece in EB welding and the use of this measured value data in adjusting the beam current and welding power used in EB welding. Austenitic stainless steel was used as the base material in the welding tests performed in the studies. The plate thickness to be welded in the studies ranged

Fig. 19 Above: Appearance from the root side of test piece 10D8. Below: weld macro cross-sections from the test piece 10D8. Cross-Section 4 is taken from the front part (thickness = 10 mm) of test piece. Cross-Section 5 is taken from in the middle part (thickness = 9 mm) of test piece and cross-Section 6 is taken from the tail part (thickness = 8 mm)
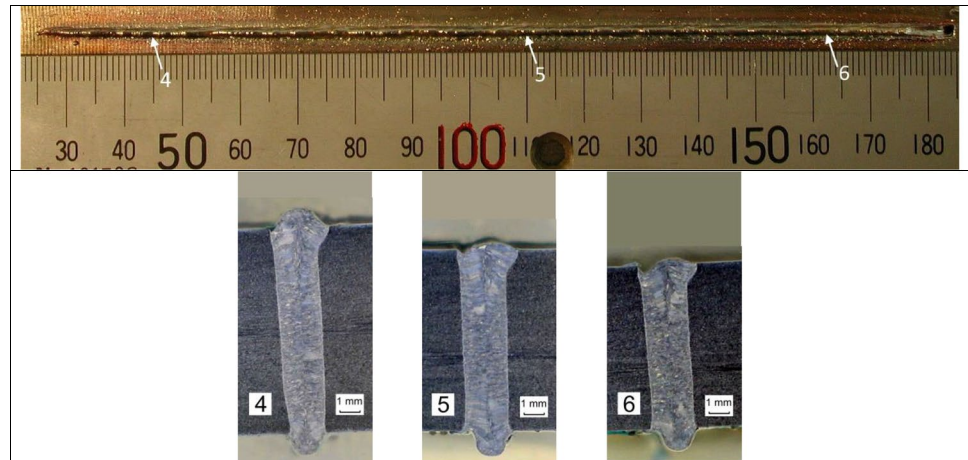
from 7 to 14 mm. The research and development process were addressed in two phases. In the first phase, a proper measurement system was developed and built. At this point, preliminary welding tests were performed to describe the sensitivity of the process and to ensure the functionality of the measurement system. The measures in the second phase were based on the promising results of the preliminary welding tests carried out in the first phase. In the second phase, the measurement system was upgraded by building a closed-loop adaptive control connection to the system. As a final part of the second phase, bead-on-plate welding tests at the flat position were performed to investigate the performance and usability of the control system developed. The following conclusions can be drawn from the results of the research carried out in this study:

- With the experimental arrangement used in the study, the electron-generated through-current was successfully measured and this measurement data could be used in a control system that regulates the required beam current and welding power depending on the plate thickness to be welded.
- It was found that the level of through-current generated by the electrons passing through the keyhole in the work piece during welding should be high enough to ensure complete penetration and smooth shape of the root side of the weld. For the welding parameters used in the tests and the austenitic stainless steel base material tested, the correlation between through-current and the thickness of the plate to be welded was determined as follows: for a plate thickness of 7 mm the minimum through-current threshold should be 0.65 mA and for plate thicknesses 10 to 14 mm the threshold level should be at least 2 mA.
- In welding tests evaluating the performance of the control system for samples where the thick-

ness of the plate to be welded changed as welding progressed, it was found that in the test run where the thickness of the sample was linearly increased from 10 to 12 mm, the control system was able to react and regulate the through-current and welding power required for complete root penetration along the entire abovementioned thickness range. In the test run, in which the thickness of the sample decreased linearly from 10 to 8 mm, the control system reacted by keeping the welding power almost constant, as the measured through-current indicated that the required threshold level was reached over the entire plate thickness range and was sufficient to enable welding conditions for complete root penetration.

- As a whole, the results of the welding tests performed showed the functionality of the developed control system and the suitability of the concept itself. However, further work is recommended, mainly to improve system reliability by collecting test data to validate adjustment limits (through-current vs. beam current) for welding tests using longer weld joints in conjunction with different welding positions and plate thicknesses.

Declarations

References

1. Schultz H (ed) (1993) Woodhead Publishing series in welding and other joining technologies. Electron Beam Welding, Woodhead Publishing, Pages vii-viii. https://doi.org/10.1016/B978-1-85573-050-2.50004-X

2. Mladenov GM, Petrov PI (1999) Physical and thermal processes during electron beam welding. Mater Manuf Process 14(3):331–345. https://doi.org/10.1080/10426919908914831

3. Węglowski MST, Błacha S, Phillips A (2016) Electron beam welding – techniques and trends – Review. Vac 130:72–92. https://doi.org/10.1016/j.vacuum.2016.05.004

4. Sarafan S, Wanjara P, Gholipour J, Champliaud H (2016) Global and local characteristics of an autogenous single pass electron beam weld in thick gage UNS S41500 steel. Materials Science and Engineering: A 666:360–371. https://doi.org/10.1016/j.msea.2016.04.044

5. Hiroki O et al (2009) Welding of metallic foil with electron beam. J Solid Mech Mater Eng 3(4):2009

6. Fang Yong-jian et al (2018) Microstructure and mechanical properties of electron beam-welded joints of titanium TC4 (Ti-6Al-4V) and kovar (Fe-29Ni-17Co) alloys with Cu/Nb multi-interlayer. Adv Mater Sci Eng 2018(2042871):11. https://doi.org/10.1155/2018/2042871

7. Saha TK, Ray AK (2008) International symposium on 'Vacuum Science and Technology' (IVS 2007) 28–30 November 2007, Tata Institute of Fundamental Research, Mumbai, India. J Phys: Conf Ser 114:012047. https://doi.org/10.1088/1742-6596/114/1/012047

8. Gupta RK et al (2018) Electron beam welding study of grade 1 CP Titanium. Mater Today: Proc 5(2018):8464–8470

9. Sang S, Li D, Wang C, Ding L, Tang Y, Xiong Q (2019) Microstructure and mechanical properties of electron beam welded joints of tantalum and GH3128. Mater Sci Eng: A 768:138431. https://doi.org/10.1016/j.msea.2019.138431

10 Badgujar BP (2017) An investigation of electron beam welding of Nb-1Zr-0.1C alloy: process parameters and microstructural analysis. J Manuf Process 28(2017):326–335. https://doi.org/10.1016/j.jmapro.2017.07.001

11. Mendez PF, Eagar TW (2001) Welding processes for aeronautics. Adv Mater Processes, May 2001, pp. 39-43 [web document]. [Retrieved July 11, 2022]. Available at: https://eagar.mit.edu/publications/Eagar184.pdf

12. Anderson G (1963) Electron Beam welding of large aerospace structures with portable vacuum chambers. SAE Tech Pap 630250:1963. https://doi.org/10.4271/630250

13. Li MF, Zhu ZH (2015) Features and application of electron beam welding technology. Advanced Materials Research 1120–1121:1308–1312. Trans Tech Publications, Ltd. https://doi.org/10.4028/www.scientific.net/amr.1120-1121.1308

14. Powers D, Schubert G (2000) Electron beam welding: a useful tool for the automotive industry. Weld J 79(2):35–38

15. Colegrove R, Carroll M (1985) EBW system for fully automatic welding of large, heavy section pieces. Proc Conf Laser vs Electron Beam Weld, Cut Surf Treat, State of the Art - 1985:97–109

16. Powers DE, Electron beam materials processing (2012) Industrial accelerators and their applications, pp 57–86. https://doi.org/10.1142/9789814307055_0003

17. Messler JR RW (1981) Electron beam weldability of advanced titanium alloys. Weld J, Weld Res Suppl, May 1981, 79s–84s

18. Feng G et al (2021) Comparison of welding residual stress and deformation induced by local vacuum electron beam welding and metal active gas arc welding in a stainless steel thick-plate joint. J Mater Res Technol, Volume 13, 2021, Pages 1967–1979, ISSN 2238–7854, https://doi.org/10.1016/j.jmrt.2021.05.105.

19. Martín-Menéndez C, Rodríguez E, Ottolini M, Caixas J, Guirao J (2016) Analysis of the effectof the Electron-Beam welding sequence for a fixed manufacturing route using finite element simulations applied toITER vacuum vessel manufacture. Fusion Engineering and Design 104:84–92. https://doi.org/10.1016/j.fusengdes.2016.02.029

20. Ji H, Xia X, Wu J, Wu H, Liu Z, Ma J, Liu Z, Shen X (2019) Welding technology development for the fabrication of vacuum vessel for CFETR. Fusion Eng Des 147:111272. https://doi.org/10.1016/j.fusengdes.2019.111272

21. Liu Z et al (2019) The key technology research of electron beam welding in CFETR vacuum vessel collar. Fusion Engineering and Design, 139: 14–18, ISSN 0920–3796, https://doi.org/10.1016/j.fusengdes.2018.12.059.

22. Buddu RK, Chauhan NL, Raole PM (2017) Investigations of microstructure and mechanical properties of 60-mm-thick type 316L stainless steel welded plates by multipass tungsten inert gas welding and electron beam welding for fusion reactor applications. Fusion Sci Technol 65(2):248–254. https://doi.org/10.13182/FST13-662

23. Ji H et al (2022) Numerical analysis of electron beam welding deformation for the vacuum vessel lower port stub of 316L stainless steel. Met 12:224. https://doi.org/10.3390/met12020224

24. Nishimura A (2019) Study on buttweld joint of thick plate superconducting coil structure to reduce welding residual deformation. Plasma Fusion Res 14(22019):3405062. https://doi.org/10.1585/pfr.14.3405062

25. Druzhinina AA et al (2022) A new control method of the joint position at the working current at electron beam welding. Weld Int 36(3):187–191. https://doi.org/10.1080/09507116.2022.2033443

26. Sizov M, Starostenko AA, Tsyganov AS, Medvedev AM (2020) Real time control system architecture for industrial electron beam welding facility based on FPGA. In Proceedings of the 2nd International Conference on Industrial Control Network and System Engineering Research (ICNSER2020). Association for computing machinery, New York, NY, USA, 1–4. https://doi.org/10.1145/3411016.3411017

27. Oltean S-E (2018) Strategies for monitoring and control with seam tracking in electron beam welding. Procedia Manufacturing 22:605–612. https://doi.org/10.1016/j.promfg.2018.03.088

28. Trushnikov D, Krotova E, Koleva E (2016) Use of a secondary current sensor in plasma during electron-beam welding with focus scanning for process control. J Sens 2016(5302681):13. https://doi.org/10.1155/2016/5302681

29. Trushnikov D, Mladenov G, Belenky V (2013) Controlling the electron beam focus regime and monitoring the keyhole in

electron beam welding. Q J Jpn Weld Soc 31:91s–95s. https://doi.org/10.2207/qjjws.31.91s

30. Oltean SE, Abrudean M (2008) Advanced control of the electron beam welding. J Control Eng Appl Informa 10(1):40–48

31. Laptenov VD, Murygin AV, Tikhonenko DV (2006) X-ray sensor for guiding the electron beam on the joint in electron-beam welding. Weld Int 20(11):894–900. https://doi.org/10.1533/wint.2006.3709

32 Shvalev A, Semenov EI (2004) Methods of guiding an electron beam on a joint between the weld edges. Weld Int 18(7):565–572. https://doi.org/10.1533/wint.2004.3329

33. Druzhinina AA, Laptenok VD, Murygin AV, Petrenko VE (2018) A method of measuring the depth of the penetration channel during electron-beam welding. Paper presented at the IOP Conference Series: Materials Science and Engineering 450(3). https://doi.org/10.1088/1757-899X/450/3/032002